

Time evolution of localized solutions in 1-dimensional inhomogeneous FPU models

F. Martínez-Farías^{1,a} and P. Panayotaros²

¹ Energetic Systems and Advanced Materials, Escuela Superior de Apan, Universidad Autónoma del Estado de Hidalgo, Carretera Apan-Calpulalpan Km. 8, Col Chimalpa, Apan 43920, Hidalgo, Mexico

² Depto. Matemáticas y Mecánica, Instituto de Investigaciones en Matemáticas Aplicadas y Sistemas, Universidad Nacional Autónoma de México, 01000 México D.F., Mexico

Received 21 December 2017

Published online 4 October 2018

Abstract. We study energy localization in a quartic FPU model with spatial inhomogeneity corresponding to a site-dependent number of interacting neighbors. Such lattices can have linear normal modes that are strongly localized in the regions of high connectivity and there is evidence that some of these localized modes persist in the weakly nonlinear regime. The present study shows examples where oscillations can remain localized for long times. Nonlinear normal modes are approximated by periodic orbits that belong to an invariant subspace of a Birkhoff normal form of the system that is spanned by spatially localized modes [F. Martínez-Farías et al., Eur. Phys. J. Special Topics **223**, 2943 (2014), F. Martínez-Farías et al., Physica D **335**, 10 (2016)]. The invariant subspace is suggested by the dispersion relation and also depends on the overlap between normal modes. Numerical integration from the approximate normal modes suggests that spatial localization persists over a long time in the weakly nonlinear regime and is especially robust in some disordered lattices, where it persists for large, $O(1)$, amplitude motions. Large amplitude localization in these examples is seen to be recurrent, i.e. energy flows back and forth between the initial localization region and its vicinity.

1 Introduction

We present a numerical study of energy localization in a spatially inhomogeneous Fermi–Pasta–Ulam (FPU) lattice with quartic inter-particle potential energy. Spatial inhomogeneity is introduced by making the number of neighbors interacting with each site depend on the site. The system was originally proposed [5,6] in [1,2] as a simplification of elastic network models for protein vibrations [3,4]. Linear elastic networks can reproduce some features of the protein vibrational spectrum [5,6]. FPU lattices with similar inhomogeneity can also model small amplitude relative phase oscillations in conservative electrical power networks [7].

^a e-mail: francisco.martinez@uaeh.edu.mx

One of the questions in biomolecular applications is the existence of spatially localized motions, and in [1,2] we proposed a general weakly nonlinear theory for such motions, based on the idea of continuing spatially localized linear normal modes. Spatial localization of normal modes is the result of inhomogeneity and can be verified numerically. The nonlinear theory uses a normal form argument to eliminate a class of nonresonant quartic mode interactions and then identify periodic orbits in invariant subspaces spanned by spatially localized modes. Despite the evidence for such nonlinear normal modes in 1-D and 3-D lattices [2] the mathematical theory is still incomplete and this motivates further analysis of simpler 1-D geometries, especially lattices that have some connectivity features of the lattices modeling biomolecules. Another open question is the stability of the approximate nonlinear modes, especially the ones that are orbitally stable in the invariant subspace [2]. We note that spectral localization for the homogeneous 1-D FPU is widely studied [8] and better understood [9–15].

The present work addresses the stability question by integrating numerically from approximate localized states found using the normal form. We will consider three lattices exhibiting localized modes. The first is a lattice with one region of high interconnectivity considered in [1]. In that case the highest linear frequencies are separated from the rest of the spectrum by a gap, moreover the highest frequency modes are spatially localized in the high interconnectivity region [1]. This example is the simplest one exhibiting localization due to regions of high connectivity. Similar localization phenomena are seen in lattices with more high connectivity regions [2]. The normal form argument uses the frequency gap to show the persistence of localized modes in the weakly nonlinear regime. The approximate localized modes were computed numerically in [2]. Numerical integration from the vicinity of this orbit suggests that for sufficiently small amplitude the energy remains localized in the high connectivity region, with significant energy interchange between several near-resonant spatially localized normal modes. At higher amplitudes we see that the energy starts to spread outside the high connectivity region.

The other two lattices we consider have a distribution of overlapping regions of higher interconnectivity. Their masses are distributed in a “random” or “disordered” way described in Section 2. The linear spectra of these lattices have no gaps and we also see localized modes for a wider range of frequencies. Some of these features are also seen in 3-D lattices for protein models [2]. In both examples we see numerically that for small amplitudes the trajectories remain in the vicinity of the spatially localized approximate periodic orbit for long times. For higher amplitude motions we see that spatial localization persists but becomes recurrent in space, in particular, energy flows to and from the vicinity of the localized initial condition, while the trajectory continues to return to the vicinity of the localized orbit. Thus localization in the disordered lattices seems to be a more robust phenomenon than in the first example.

The paper is organized as follows. In Section 2 we present the quartic FPU lattice model and discuss linear normal modes. We present two examples of 1-D disordered FPU lattices and their spectral properties. In Section 3 we discuss normal forms and the construction of approximate nonlinear localized modes. In Section 4 we study the evolution from initial conditions that approximate nonlinear localized modes. We show examples of localization, delocalization, and recurrent localization.

2 Inhomogeneous FPU lattice model and localized linear modes

We consider the quartic Fermi–Pasta–Ulam Hamiltonian

$$\mathcal{H} = \frac{1}{2m} \sum_{i=1}^N |\mathbf{p}_i|^2 + \sum_{i,j=1}^N c_{ij} \left[\frac{k_2}{2} |\mathbf{q}_i - \mathbf{q}_j|^2 + \frac{k_4}{4} |\mathbf{q}_i - \mathbf{q}_j|^4 \right], \quad (1)$$

with position, and momentum variables $\mathbf{q}_i, \mathbf{p}_i \in \mathbb{R}^D, i = 1 \dots N$. $|\cdot|$ is the Euclidean distance in \mathbb{R}^D . The pairwise interaction among particles i, j is described by the symmetric coefficients $c_{ij}, i, j = 1 \dots N$, that are either 1 or 0. The interaction coefficients c_{ij} also determine the adjacency matrix of a graph with nodes $i = 1 \dots N$.

In the case $D = 1$ the quadratic part U_2 of the potential energy is

$$U_2 = \frac{k_2}{2} \sum_{i,j=1}^N c_{ij} (\mathbf{q}_i - \mathbf{q}_j)^2 = k_2 \langle q, Cq \rangle, \tag{2}$$

where $q = (q_1, q_2, \dots, q_N)$, $\langle \cdot, \cdot \rangle$ denotes the Euclidean inner product in \mathbb{R}^N , and C is

$$C = \begin{pmatrix} n_1 & -c_{21} & \dots & -c_{N1} \\ -c_{12} & n_2 & \ddots & \vdots \\ \vdots & \ddots & n_{N-1} & -c_{NN-1} \\ -c_{1N} & \dots & -c_{N-1N} & n_N \end{pmatrix}, \tag{3}$$

where n_j is the number of sites $i \neq j$ that interact with the site j . Therefore $C = -\Delta$, Δ the Laplacian of the graph defined by the c_{ij} .

The quartic FPU model (1) with $k_2, k_4 > 0$ was derived from an elastic lattice model for protein vibrations [2], and the \mathbf{q}_i represent the displacement from some known equilibrium configuration obtained from crystallographic data. Elastic lattices for protein vibrations are discussed in [3–5,16,17]. Sites with many interacting neighbors correspond to denser regions of the protein. The physically interesting dimension is $D = 3$, but $D = 1$ studies still capture some 3-D phenomena, for instance localized linear modes [1,2] see Remark 1. The absence of cubic interactions is equivalent to imposing even symmetry near equilibria. The presence of cubic corrections is currently investigated.

The case $k_2 > 0, k_4 < 0$ ($D = 1$) occurs in a small amplitude, conservative version of interacting rotors that model electrical generators and motors in an electric grid [7]. In that work $\mathbf{q}_i = \theta_i$ represents the angle (phase) of the rotor at site i . The proposed intersite interaction is $\sin(\theta_i - \theta_j)$ between rotors i, j . Taylor expanding up to cubic terms around the fully synchronized state where all phases are equal leads to the quartic FPU Hamiltonian (1).

In what follows we consider the $D = 1$ case, generalizations to higher dimension are discussed in [2]. Let $p = (p_1, p_2, \dots, p_N)$, $q = (q_1, q_2, \dots, q_N)$. Linear normal modes are obtained by diagonalizing C . The eigenvalues of C are $0 = \lambda_1 < \lambda_2 \leq \dots \leq \lambda_N$. $\Lambda = \text{diag}\{\lambda_1, \dots, \lambda_N\}$ satisfies $C = M\Lambda M^T$, with M is the orthogonal matrix of eigenvectors of C . Using the symplectic change variables $P = Mp$, $Q = Mq$, and the conservation of P_1 , see [1,2], we can consider Hamilton's equations for $Q_2 \dots Q_N$ and $P_2 \dots P_N$, and the Hamiltonian

$$\mathcal{H} = \frac{1}{2m} \sum_{l=2}^N P_l^2 + k_2 \sum_{l=2}^N \lambda_l Q_l^2 + \frac{k_4}{4} \sum_{l_1, l_2, l_3, l_4=2}^N \Gamma_{l_1 l_2 l_3 l_4} Q_{l_1} Q_{l_2} Q_{l_3} Q_{l_4}, \tag{4}$$

where

$$\Gamma_{l_1 l_2 l_3 l_4} = \sum_{i,j=1}^N c_{ij} (M_{il_1} - M_{jl_1})(M_{il_2} - M_{jl_2})(M_{il_3} - M_{jl_3})(M_{il_4} - M_{jl_4}). \tag{5}$$

We also introduce normal mode variables by letting $Q'_l = \sqrt{m}Q_l$, $P'_l = \frac{1}{\sqrt{m}}P_l$, and

$$a_l = \sqrt{\frac{\omega_l}{2}}Q'_l + \frac{i}{\sqrt{2\omega_l}}P'_l, \quad a_l^* = \sqrt{\frac{\omega_l}{2}}Q'_l - \frac{i}{\sqrt{2\omega_l}}P'_l, \quad (6)$$

with

$$\omega_l = \sqrt{\frac{2k_2\lambda_l}{m}}, \quad l = 2, \dots, N. \quad (7)$$

Then the Hamiltonian becomes

$$\begin{aligned} \mathcal{H} = & \sum_{k=2}^N \omega_k a_k a_k^* + \frac{k_4}{4} \sum_{k_1, k_2, k_3, k_4=2}^N \tilde{\Gamma}_{k_1 k_2 k_3 k_4} \left[a_{k_1} a_{k_2} a_{k_3} a_{k_4} + 4a_{k_1} a_{k_2} a_{k_3} a_{k_4}^* \right. \\ & \left. + 6a_{k_1} a_{k_2} a_{k_3}^* a_{k_4}^* + 4a_{k_1} a_{k_2}^* a_{k_3}^* a_{k_4}^* + a_{k_1}^* a_{k_2}^* a_{k_3}^* a_{k_4}^* \right], \end{aligned} \quad (8)$$

with

$$\tilde{\Gamma}_{k_1 k_2 k_3 k_4} = \frac{\Gamma_{k_1 k_2 k_3 k_4}}{4\sqrt{\omega_{k_1} \omega_{k_2} \omega_{k_3} \omega_{k_4}}}. \quad (9)$$

The ω_l are the frequencies of the linear normal modes, (7) shows their relation to the eigenvalues of $C = -\Delta$.

We construct examples of 1-D chains by considering points \mathbf{R}_i , $i = 1, \dots, N$, on the line, fixing some $R_c > 0$, and setting $c_{i,j} = c_{j,i} = 1$ if $|\mathbf{R}_i - \mathbf{R}_j| \leq R_c$ and $c_{i,j} = c_{j,i} = 0$ otherwise. R_c is such that each i interacts with at least the first j immediately to its right and left (i.e. its “nearest neighbors”).

The standard nearest-neighbor FPU can be constructed by considering equidistant \mathbf{R}_i and a suitable R_c . Adding more points \mathbf{R}_j introduces connections with more neighbors. In [1,2] we considered chains with one and up to three such “agglomeration” regions and saw that the highest frequency modes are strongly localized precisely in these regions [1,2].

The simplest examples have one region of higher connectivity, e.g. Example 1 of [1,2]. The highest frequencies are separated by the rest of the spectrum by a gap, and the corresponding modes are localized in the higher connectivity region [1,2]. Recall that the spectrum of C for the fully connected graph of n sites consists of two eigenvalues 0, and $n + 1$, of multiplicities 1, and $n - 1$ respectively. Also, the highest eigenvalue of C for the nearest-neighbor chain is 4. In the case of one agglomeration region of size n , we observe that the frequency gap is approximately proportional to $\sqrt{n + 1} - 2$, see (7). Adding smaller agglomeration regions fills the gap but we still have modes localized in the new agglomeration regions.

In this work we consider new examples generated by randomizing the distributions of the \mathbf{R}_i . This results in more agglomeration regions, of different sizes, and with possible overlaps. (Absence of overlaps means absence of tridiagonal segments in C .) The spectrum of C is visualized by plotting the “dispersion relation” ω_l vs. l , where the generalized “wavenumber” l is an index enumerating the frequencies in increasing order. The eigenfunctions of C for the 1-D models are shown in Figures 2a and 5a. We plot the absolute value of the entries of the matrix of eigenvalues M vs. indices l, i , where $M_{i,l}$ is the value of the i th entry of the l th eigenvector of C . (This is also the amplitude of q at site i for the l th eigenmode.) l enumerates the eigenvalues in increasing order.

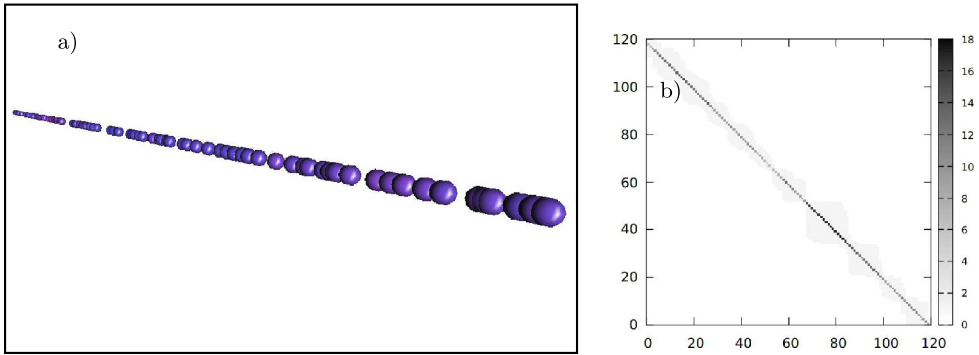


Fig. 1. Example 1. (a) 1-D chain of $N = 120$ particles with agglomeration zones of different sizes. (b) Visual representation of the connectivity matrix, the scale represents the number of neighbors.

Example 1. $D = 1$, $N = 120$: the points \mathbf{R}_j for this chain were obtained by letting $\mathbf{R}_1 = 0$, and then adding points to the right of the origin. The distance $\mathbf{R}_{j+1} - \mathbf{R}_j$ is a pseudo-random number between 0.01 and 0.35, obtained using the Mersenne Twister method (with period of $2^{19937} - 1$), [18], implemented in Octave [19]. This leads to a point distribution with several agglomeration zones, see Figure 1a, and to blocks of different sizes in the connectivity matrix, see Figure 1b. The dispersion relation in Figure 2a indicates no frequency gaps. Figure 2b indicates the existence of several localized modes. This is seen more clearly in Figure 3, where we see examples of two high frequency modes. The largest agglomeration region in this example has 11 sites.

Example 2. $D = 1$, $N = 120$: the points \mathbf{R}_j for this chain were produced by letting $\mathbf{R}_1 = 0$, and then adding points to the right. The distance $\mathbf{R}_{j+1} - \mathbf{R}_j$ is a pseudo-random number from a normal (Gaussian) distribution with mean 0.5 and standard deviation 0.2, see [20] for algorithm, this is also implemented in Octave [19]. This leads to a point distribution with several agglomeration zones, see Figure 4a, and to blocks of different sizes in the connectivity matrix, where some particles interact with up to six neighbors, see Figure 4b. Figures 5a and 5b show the dispersion relation and eigenfunctions respectively. The existence of localized modes is seen more clearly in Figure 6, where we plot two high frequency modes which correspond to the regions of greater agglomeration of this example.

Remark 1. The main similarities of the above examples with the 3-D protein models in [2,21] are the lack of frequency gaps and the existence of localized modes. Also, the relative size of the agglomeration regions is comparable to what we see in the protein examples, e.g. ~ 40 sites (out of a total of ~ 850 sites) for the protein (Ribozyme) model of [2].

3 Approximate nonlinear normal modes

The persistence of the numerically observed spatially localized normal modes for the nonlinear problem was investigated in [1,2] using Birkhoff normal forms. There are two versions of the normal form argument, both leading to a quartic normal form with an invariant subspace spanned by the high frequency, spatially localized motions. A further global phase symmetry in the high frequency subspace of the normal form allows us to show the existence of periodic orbits that are orbitally stable in the invariant subspace. These orbits are our semi-analytic approximations of nonlinear normal modes that are also spatially localized.

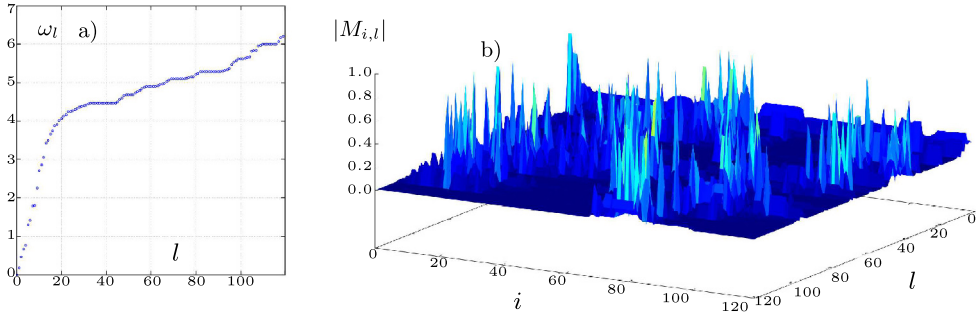


Fig. 2. Example 1. (a) Frequency ω_l vs. mode index l (dispersion relation). In this example there are no gaps at high frequencies. (b) Eigenmode $M_{i,l}$ at site i of l th eigenvalue vs. l . Spatially localized solutions are observed for a wide frequency range.

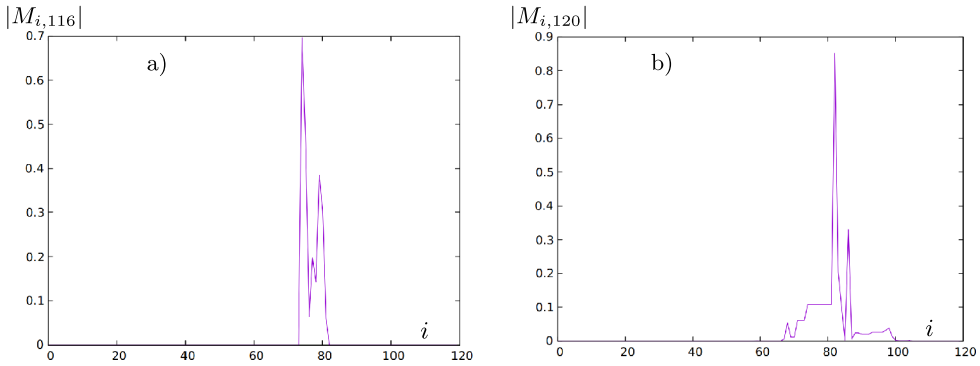


Fig. 3. Example 1. Spatial localization of some high frequency modes, (a) eigenfunction associated with the 116th mode, (b) eigenfunction associated with 120th mode, the highest frequency mode.

The first version of this construction is motivated by examples where we have a frequency gap between high and low frequencies and the high frequency modes are spatially localized, e.g. Example 1 of [1,2]. We assume there exist disjoint sets of indices $\mathcal{I}_-, \mathcal{I}_+, \mathcal{I}_- \cup \mathcal{I}_+ = \{2, \dots, N\}$, so that letting

$$\omega_c = \max_{j \in \mathcal{I}_-}(\omega_j), \quad \Omega_c = \min_{j \in \mathcal{I}_+}(\omega_j), \tag{10}$$

we have $\omega_c < \Omega_c$. Also letting

$$G = \Omega_c - \omega_c, \quad \Delta = \max_{i,j \in \mathcal{I}_+} |\omega_i - \omega_j|, \quad i, j \in \mathcal{I}_+, \tag{11}$$

we assume

$$\Omega_c - \Delta \geq O(1), \quad G \geq O(1), \quad G - \Delta \geq O(1). \tag{12}$$

The notation $O(1)$ assumes that there is a small parameter in the problem, e.g. the smallest nontrivial frequency ω_2 of the chain, so that $O(1)$ means independent of ω_2 . This notion becomes well defined when the chains are extended to arbitrary size from both sides, with nearest neighbor interactions in the extensions. $O(1)$ quantities are the ones that are expected to approach a nonzero constant in the limit.

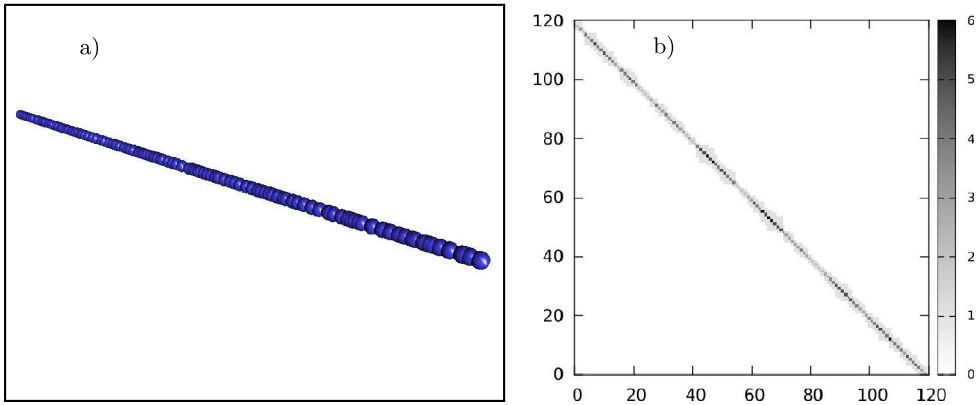


Fig. 4. Example 2. 1-D chain of $N = 120$ particles. (a) Visualization of the random chain. (b) Visual representation of the connectivity matrix, the scale represents the number of neighbors.

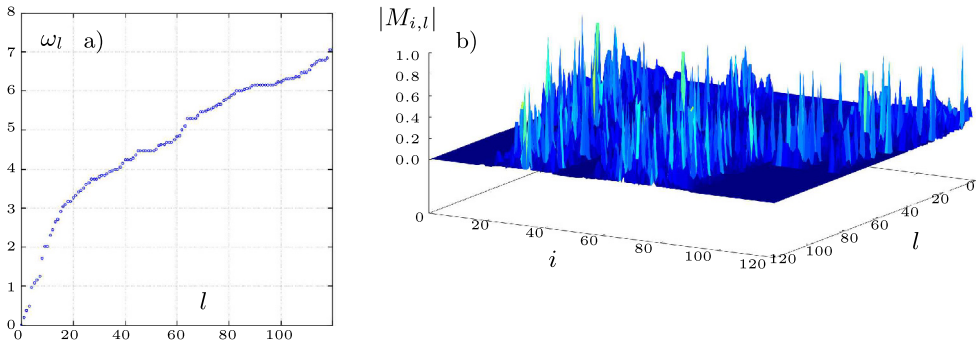


Fig. 5. Example 2. (a) Frequency ω_l vs. mode index l (dispersion relation). (b) Eigenmode $M_{i,l}$ at site i of l th eigenvalue vs. l . Spatially localized solutions are observed for a wide frequency range.

The existence of a quartic normal form with an invariant subspace is stated as follows, see [1,2]. We start with the Hamiltonian $\mathcal{H} = \mathcal{H}_2 + \mathcal{H}_4$ of (8), with $\mathcal{H}_2, \mathcal{H}_4$ the quadratic and quartic parts respectively.

Proposition 1. *We can define a symplectic change of coordinates to new variables $a = f(\tilde{a})$, $a = \tilde{a} + \text{cubic terms}$, $a = (a_2, \dots, a_N)$ (new variables), $\tilde{a} = (\tilde{a}_2, \dots, \tilde{a}_N)$ (original variables), that is generated by a function*

$$S = \sum_{\mathcal{M} \in \mathcal{J}} S_{\mathcal{M}}, \tag{13}$$

where the $S_{\mathcal{M}}$ are quartic monomials of the form

$$S_{\mathcal{M}} = \frac{i\tilde{\Gamma}_{k_1 k_2 k_3 k_4}}{\sum_i^4 \sigma(k_i)\omega_{k_i}} b_{k_1} b_{k_2} b_{k_3} b_{k_4}, \tag{14}$$

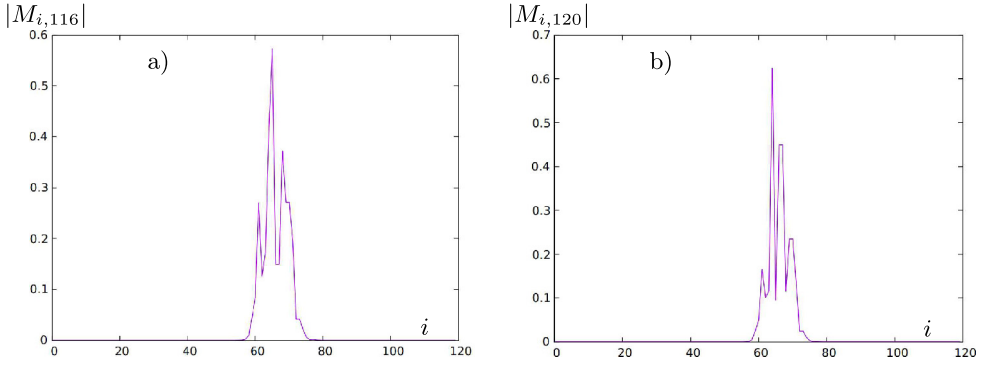


Fig. 6. Example 2. Spatial localization for some high frequency modes, (a) eigenfunction associated with the 116th mode, (b) eigenfunction associated with 120th mode, the highest frequency mode.

$b_k = a_k$ or a_k^* , and $\sigma_k = 1$ if $b_k = a_k$, -1 if $b_k = a_k^*$, that satisfy $\sum_{i=1}^4 \sigma(k_j)\omega_{k_i} \geq O(1)$. Moreover the Hamiltonian in the new coordinates has the form $\tilde{\mathcal{H}} = \mathcal{H}_2 + \tilde{\mathcal{H}}_4 + O(6)$, where

$$\tilde{\mathcal{H}}_4 = \mathcal{H}_4 + [\mathcal{H}_2, S], \tag{15}$$

and $O(6)$ represents terms of order six and higher, and satisfies that

- (i) the subspace V_+ defined by $a_j = 0, \forall j \in \mathcal{I}_-$, is invariant under the Hamiltonian flow of the quartic normal form $\tilde{\mathcal{H}} = \mathcal{H}_2 + \tilde{\mathcal{H}}_4$, and
- (ii) the quartic Hamiltonian $\tilde{\mathcal{H}}$, restricted to V_+ , is invariant under the action $a_j \mapsto a_j e^{i\phi}$, for all $j \in \mathcal{I}_+, \phi \in \mathbb{R}$.

In the examples where the gap separating low and high frequency modes becomes smaller, see [2], or is absent, as in Examples 1, 2 of Section 2, the bounds in part (i) of Proposition 1 can not hold because (12) fails.

On the other hand, the observation of normal modes localized in different regions in the examples of [2] and in Examples 1, 2 suggests that the numerators $\tilde{\Gamma}_{k_1 k_2 k_3 k_4}$ in (14) can be small when we are close to some resonances, so that the coefficient of the monomial $\mathcal{S}_{\mathcal{M}}$ remains small.

To examine this scenario we decompose the set of frequencies into three sets of “low”, “medium”, and “high” frequency modes, with respective index sets $\mathcal{I}_-, \mathcal{I}_m, \mathcal{I}_+$. The sets $\mathcal{I}_-, \mathcal{I}_m, \mathcal{I}_+$ are mutually disjoint, with $\mathcal{I}_- \cup \mathcal{I}_m \cup \mathcal{I}_+ = \{2, \dots, N\}$. Also $i \in \mathcal{I}_-, j \in \mathcal{I}_m$ implies $i < j$, and $j \in \mathcal{I}_m, k \in \mathcal{I}_+$ implies $j < k$.

Given such a decomposition we define E_k by

$$E_k = \max_{k_2, k_3, k_4 \in \mathcal{I}_+} \left\{ \max_{\sigma(j) = \pm 1} \left| \frac{\tilde{\Gamma}_{k k_2 k_3 k_4}}{\sum_{j=1}^4 \sigma(k_j)\omega_{k_j}} \right| \right\}, \quad k \in \mathcal{I}_- \cup \mathcal{I}_m. \tag{16}$$

We also define \tilde{E} as

$$\tilde{E} = \max_{k \in \mathcal{I}_- \cup \mathcal{I}_m} \{E_k\}. \tag{17}$$

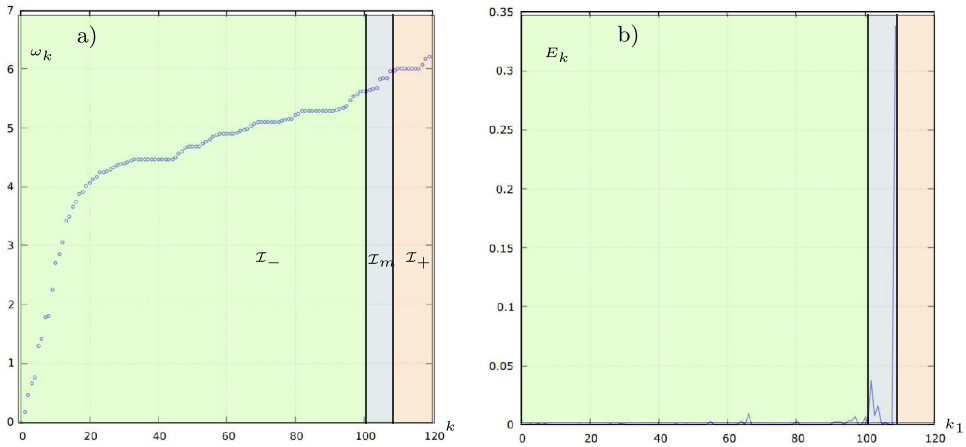


Fig. 7. (a) Dispersion relation of Example 1 and decomposition into low, medium, and high modes, \mathcal{I}_- , \mathcal{I}_m , \mathcal{I}_+ respectively. (b) E_k with $k \in \{2, \dots, 109\}$ y $k_2, k_3, k_4 \in \{110, \dots, 120\}$. E_k is negligible for $k \in \mathcal{I}_-$, larger values are seen for $k \in \mathcal{I}_m$.

In (16) note that the coefficients $\tilde{\Gamma}_{kk_2k_3k_4}$ are invariant under permutations of the subindices. Also, $\max_{\sigma(j)=\pm 1}$ denotes the maximum over all combinations of the signs $\sigma(k_j)$ in the frequency sum appearing in the denominator.

The decomposition into low, medium, and high modes is arbitrary. We try different choices of \mathcal{I}_- , \mathcal{I}_m , \mathcal{I}_+ and check that E_k , and \tilde{E} remain under some value. At the same time we check that modes in \mathcal{I}_+ have spatial localization.

Example 1. It is not obvious how to divide the modes of the dispersion relation of Figure 7a. One possible way is to look for k where E_k changes abruptly. For instance, consider k in the interval $\{2, \dots, 109\}$, and $k_2, k_3, k_4 \in \{110, \dots, 120\}$. Figure 7b indicates that E_k remains less than 10^{-1} when $k \leq 101$, and starts to grow just passing this value. This indicates that we have left \mathcal{I}_- and are in the range of modes in \mathcal{I}_m . The interaction continues to increase, reaching $E_k = 10^0$ when we consider $k = 110$. We then choose $\mathcal{I}_- = \{2, \dots, 102\}$, $\mathcal{I}_m = \{102, \dots, 109\}$, and $\mathcal{I}_+ = \{110, \dots, 120\}$, and obtain $\tilde{E} < 0.35$.

Example 2. We follow the same procedure as in the example above and choose the same decomposition $\mathcal{I}_- = \{2, \dots, 102\}$, $\mathcal{I}_m = \{102, \dots, 109\}$, and $\mathcal{I}_+ = \{110, \dots, 120\}$, with $\tilde{E} < 0.93$.

The invariant subspace statement for the quartic normal form is as follows.

Proposition 2. *There exists a symplectic change to new variables $a = f(\tilde{a})$, where $a = \tilde{a} +$ cubic terms (new variables), and $a = (a_2, \dots, a_N)$, $\tilde{a} = (\tilde{a}_2, \dots, \tilde{a}_N)$ (old variables), that is generated by a function \mathcal{S} as in (13) that is the sum of monomials \mathcal{S}_M of the form (14), and has coefficients satisfying either*

$$\frac{\tilde{\Gamma}_{k_1k_2k_3k_4}}{\sum_{j=1}^4 \sigma(k_j)\omega_j} \leq \tilde{E},$$

or $\sum_{j=1}^4 \sigma(k_j)\omega_j \geq 2\Omega_c - \Delta$, Ω_c , Δ as in (10), (11), such that

- (i) the subspace V_+ defined by $a_j = 0$, for all $j \in \mathcal{I}_- \cup \mathcal{I}_m$, and $d \in \{1, \dots, D\}$, is invariant under the Hamiltonian flow of the quartic normal form $\tilde{\mathcal{H}} = \mathcal{H}_2 + \tilde{\mathcal{H}}_4$, $\tilde{\mathcal{H}}_4$ as in (15), and

(ii) the quartic Hamiltonian $\bar{\mathcal{H}}(a)$, restricted to V_+ , is invariant under the action $a_j \mapsto a_j e^{i\phi}$, for all $j \in \mathcal{I}_+$, and $\phi \in \mathbb{R}$.

The symmetry under global phase change in Propositions 1 (ii), 2 (ii) implies that the Hamiltonian flow of $\bar{\mathcal{H}}_+$, the restriction of $\bar{\mathcal{H}}$ to V_+ , has the additional constant of motion

$$\mathcal{P}_+ = \sum_{l \in \mathcal{I}_+} |a_l|^2. \quad (18)$$

The flow of $\bar{\mathcal{H}}_+$ then has periodic orbits of the form $a = e^{-i\lambda t} A$, $A \in V_+ = \mathbb{C}^{|\mathcal{I}_+|}$, $\lambda \in \mathbb{R}$. These orbits are often called (discrete) “breathers”, see [22]. Stable breathers in V_+ are expected to be spatially localized provided the corresponding modes are spatially localized.

The amplitude A of a breather solution is also a critical point of $\bar{\mathcal{H}}_+$ on hyperspheres $S_c = \{v \in V_+ : \mathcal{P}_+(v) = c\}$. Local extrema of $\bar{\mathcal{H}}_+$ on S_c therefore correspond to orbitally stable breathers in V_+ . However stability in the invariant subspace V_+ does not imply stability in the whole phase space. This question is addressed in the next section.

Note that extrema of $\bar{\mathcal{H}}_+$ on the S_c are computed numerically by a steepest descent algorithm (with rescaling), i.e. following numerically the gradient of $\pm \bar{\mathcal{H}}_+$ and rescaling at every time-step to maintain P constant. The method is described in [2], and we will not include details of how we compute breathers here.

4 Time evolution from breather solutions and evidence for stability

In this section we study the evolution from initial conditions that are breather solutions in the invariant subspaces V_+ for a chain with one agglomeration region, Example 1 of [1,2], and for the disordered lattices of Examples 1 and 2 of Section 2. The corresponding high frequency index sets \mathcal{I}_+ were specified in the previous section. We omit details on the computation of the breathers, see [2].

To integrate the Hamiltonian flow of the original model (1) we use the symplectic integration method PEFRL [23,24]. The integration time for all cases is $10\tau_{\max}$, where $\tau_{\max} = 2\pi/\omega_2$ is the period of the lowest frequency linear mode for each configuration. In comparison, the breather frequencies are close to the highest linear frequency ω_N . Thus the integration time is $10\omega_N/\omega_2 \tau_{\min}$, where $\tau_{\min} = 2\pi/\omega_N$ is an approximation of the period of the breather.

The spectra of the lattices considered, see e.g. Figures 2 and 5, yield $\omega_N/\omega_2 \sim 10^2$, so that the integration time used is about 10^3 times the period of the breather. Numerical conservation of energy is indicated by the quantity $(\Delta E(t))/E(0)$, where $\Delta E = E(t) - E(0)$. We integrate using the PEFRL scheme with stepsize $h = 10^{-2}$, 10^{-3} , 10^{-4} over $t = 10\tau_{\max}$ and obtain values $(\Delta E)/E(0) \sim 10^{-4}$, 10^{-6} , 10^{-9} respectively for all three examples considered. We also saw that the PEFRL method is more accurate than the simpler (third order) Storm–Verlet and Runge–Kutta (RK4) schemes [25,26].

We first consider the evolution of the breather obtained for a chain with one agglomeration region, in particular Example 1 of [2]. The number of sites is $N = 109$ and the breather was computed in [2]. The high frequency subspace is spanned by modes with index $l \in \mathcal{I}_+ = \{99, \dots, 109\}$.

The results are indicated in Figure 8 (mode space), and Figure 9 (space) for $k_4 = 0.25$, and 1.0. For $k_4 = 0.25$, Figure 8a indicates significant energy exchange between some of the modes in the high frequency set \mathcal{I}_+ , especially the modes

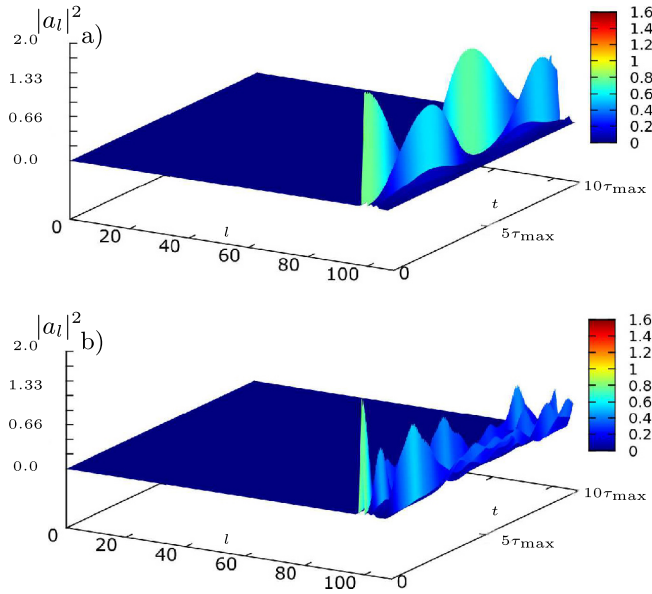


Fig. 8. Example 1 of [2]. Mode amplitude $|a_l|^2$ vs. time t , $l = 2 \dots 109$, initial condition is breather of normal form in V_+ , [2], (a) $k_4 = 0.25$ and (b) $k_4 = 1.0$.

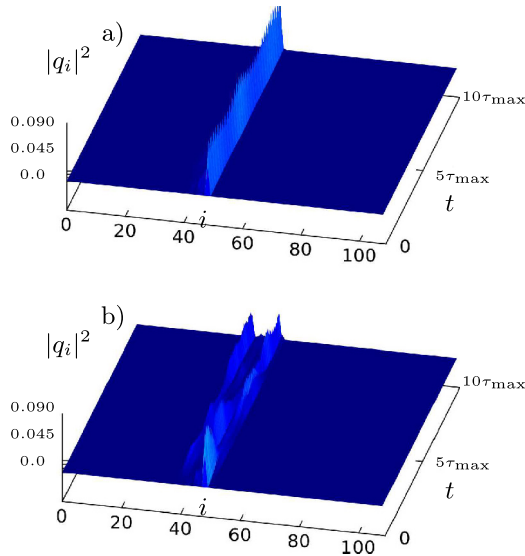


Fig. 9. Example 1 of [2]. Amplitude $|q_i|^2$ vs. time t , $l = 1 \dots 109$, initial condition is breather on V_+ : (a) $k_4 = 0.25$. (b) $k_4 = 1.0$.

with $l = 99$ and 100 . There is little energy leaking to modes with index $l < 99$. Figure 9b shows the corresponding spatially localized pattern. The highest amplitudes are observed in the agglomeration region. As we increase k_4 , energy starts to delocalize, both in space and mode space. This is indicated in Figures 8b and 9b, where $k_4 = 1.0$. In Figure 9b high amplitude motion begins to spread from the agglomeration region.

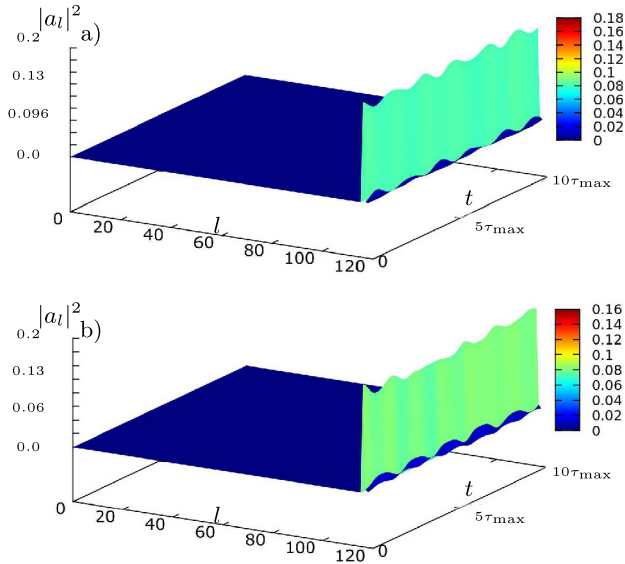


Fig. 10. Example 1, Section 2. Mode amplitude $|a_l|^2$ vs. time t , $l = 2 \dots 120$, initial condition is breather on V_+ , (a) $k_4 = 0.25$, (b) $k_4 = 1.0$.

In this example the breather is the constrained minimum of $\tilde{\mathcal{H}}_+$. In the limit $k_4 = 0$ the breather is the mode with index $l = 99$, i.e. the smallest index in \mathcal{I}_+ [2]. Increasing k_4 with fixed power changes little the shape of the breather. The strong energy interchange among some high frequency modes seen for $k_4 = 0.25$ may be related to the near degeneracy of the frequencies of the first linear modes of \mathcal{I}_+ (a related fact is that, as k_4 vanishes, there is a multidimensional subset of the constant energy supersurface where the energy variation is of $O(k_4)$). These resonance phenomena can be studied at more depth, using two or three mode truncations of the high-frequency system.

Consider now the lattice of Example 1, Section 2. In Figures 10 and 11 we see the evolution from breather initial conditions for $k_4 = 0.25$, and 1.0. Localization is considerably more robust, with most of the energy concentrated at a single mode, see Figures 10a and 10b. In particular, localization in mode space is still pronounced for $k_4 = 1$. The spatial picture, Figure 11b, indicates that for larger k_4 spatial localization becomes recurrent. Energy moves back and forth between the region of initial localization and its vicinity. The spatial pattern is due to the interchange of energy between a dominant mode and modes with nearby indices. The amount of energy interchanged is small, and not as appreciable in Figure 10, but is sufficient for the recurrent transfer of energy in space.

Example 2 of section also exhibits robust localization. Most of the energy is concentrated in a dominant mode, see Figures 12a and 12b, where we consider $k_4 = 0.25$, 1.0 respectively. Energy exchange with other modes increases with k_4 , but localization in mode space remains pronounced for $k_4 = 1$. The small amount of energy exchange has the effect of making spatial localization recurrent as k_4 increases. At $k_4 = 1$ we see that energy moves back and forth between two nearby regions, see Figure 13b.

In summary, Examples 1, 2, representing more disordered connectivities, exhibit more robust localization than the chain one region with higher connectivity considered [1,2]. In the new examples increasing k_4 has a minor effect, with linear localization being a good indicator of nonlinear behavior. As k_4 increases further to unity, localization in mode space persists. In space we see the more subtle behavior of recurrent localization.

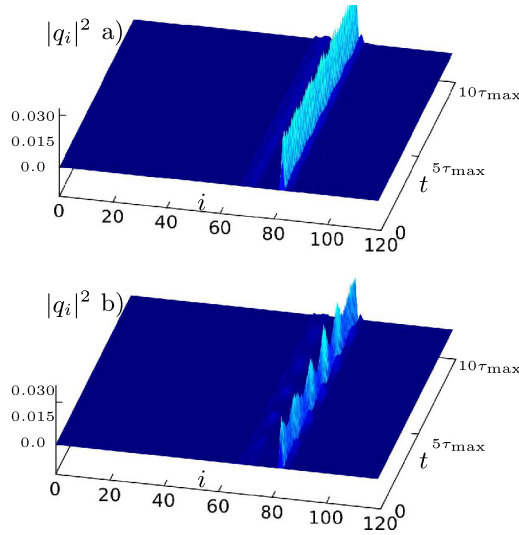


Fig. 11. Example 1, Section 2. Amplitude $|q_i|^2$ vs. time t , $i = 1 \dots 120$, initial condition is breather on V_+ , (a) $k_4 = 0.25$, (b) $k_4 = 1.0$.

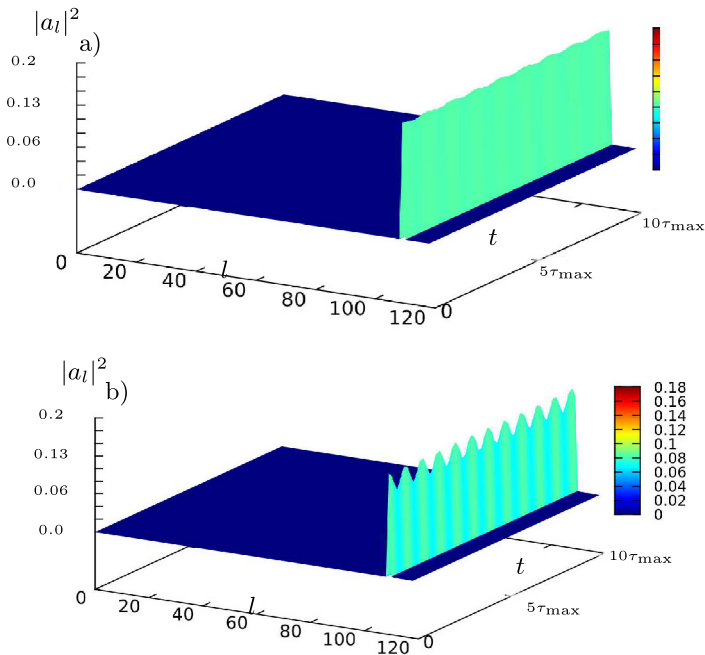


Fig. 12. Example 2, Section 2. Mode amplitude $|a_l|^2$ vs. time t , $l = 2 \dots 120$, initial condition is breather on V_+ , (a) $k_4 = 0.25$, (b) $k_4 = 1.0$.

5 Discussion

The present study examined numerically spatially localized oscillations in quartic FPU lattices with a site-dependent number of interacting neighbors. We considered an example with a single region of higher interconnectivity studied in earlier works, as

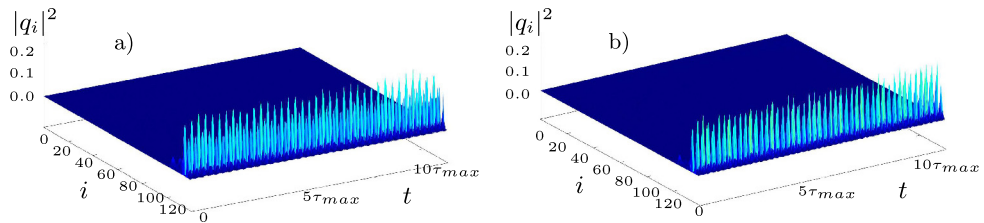


Fig. 13. Example 2, Section 2. Amplitude $|q_i|^2$ vs. time t , $i = 1 \dots 120$, initial condition is breather on V_+ , (a) $k_4 = 0.25$, (b) $k_4 = 1.0$.

well as two new examples obtained by a pseudo-random distribution of masses. In the first example, the normal form theory of localization is capable of describing qualitatively the weakly nonlinear regime. The interaction between localized modes requires further study, as there is considerable exchange of energy between several localized modes that are near-resonant. As the nonlinear interaction strength k_4 increases, the breather solution of the normal form seems less relevant. We also see a slow delocalization and the generation of waves radiating from the agglomeration region.

In the new examples, spectral and spatial localization seems to be significantly more robust, and the trajectory keeps returning to the vicinity of the breather solution of the normal form system even for $O(1)$ values of the nonlinearity parameter. Thus the linear behavior gives a good qualitative guess of localization in the nonlinear regime. This may be a consequence of randomness, which apparently causes small overlap between the normal modes. We also see the subtler effect of recurrent localization, with energy moving back and forth between the region of initial localization and nearby regions.

A more refined analysis would require a numerical computation of the periodic orbits suggested by the breather solution of the normal form. High amplitude periodic orbits for 3-D nonlinear elastic lattices for proteins were considered in [17,27], using a truncated harmonic balance, see e.g. [28] for current extensions of this method. Alternative collocation methods are reported in [29]. Nonlinear normal modes are expected to exist by the Weinstein–Moser theorem [30,31], but the main issue is their continuation from normal modes in the case of near-resonance, and the connection to spatial localization for larger amplitudes.

P.P. wishes to thank J.G. Caputo and I. Khames for helpful discussions on graph spectra. F.M. was partially supported by grant UAEH-PTC-764, DSA/511-6/17-8021.

References

1. F. Martínez-Farías, P. Panayotaros, A. Olvera, *Eur. Phys. J. Special Topics* **223**, 2943 (2014)
2. F. Martínez-Farías, P. Panayotaros, *Physica D* **335**, 10 (2016)
3. S. Nicolay, Y.H. Sanejouand, *Phys. Rev. Lett.* **96**, 078104 (2006)
4. B. Juanico, Y.H. Sanejouand, F. Piazza, P. De Los Rios, *Phys. Rev. Lett.* **99**, 238104 (2007)
5. D. ben-Avraham, M. Tirion, *Biophys. J.* **68**, 1231 (1995)
6. M. Tirion, *Phys. Rev. Lett.* **77**, 1905 (1996)
7. M. Rohden, A. Sorge, M. Timme, D. Witthaut, *Phys. Rev. Lett.* **109**, 064101 (2012)
8. F.M. Izrailev, B.V. Chirikov, *Soviet Phys. Doklady* **11**, 30 (1966)
9. C. Antonopoulos, T. Bountis, C. Skokos, *Int. J. Bifurc. Chaos* **16**, 1777 (2006)
10. D. Bambusi, A. Poincaré, *Commun. Math. Phys.* **264**, 539 (2006)

11. H. Christodoulidi, C. Euthymiopoulos, T. Bountis, *Phys. Rev. E* **81**, 016210 (2010)
12. H. Christodoulidi, C. Euthymiopoulos, *Physica D* **261**, 93 (2013)
13. S. Flach, A. Ponno, *Physica D* **237**, 908 (2007)
14. T. Genta, A. Giorgilli, S. Paleari, T. Penati, *Phys. Lett. A* **376**, 2038 (2012)
15. A. Henrici, T. Kappeler, *J. Eur. Math. Soc.* **11**, 1025 (2009)
16. D. ben-Avraham, M. Tirion, *Physica A* **249**, 415 (1998)
17. F. Piazza, Y.H. Sanejouand, *Discret. Contin. Dyn. Syst. S* **4**, 1247 (2011)
18. M. Matsumoto, T. Nishimura, *ACM Trans. Model. Comput. Simulation* **8**, 3 (1998)
19. J.W. Eaton, D. Bateman, S. Hauberg, R. Wehbring, 2016 GNU Octave version 4.2.2 manual: a high-level interactive language for numerical computations, <http://www.gnu.org/software/octave/doc/interpreter>
20. J. Ahrens, U. Dieter, *Math. Comput.* **27**, 927 (1973)
21. F. Martínez-Farías, Ph.D. Thesis, UNAM, 2016
22. J.C. Eilbeck, P.S. Lomdahl, A.C. Scott, *Physica D* **16**, 318 (1985)
23. P. Young, (2014), Available at: <http://young.physics.ucsc.edu/115/> (accessed 2017/5/12)
24. I.P. Omelyan, I.M. Mryglod, R. Folk, *Comput. Phys. Commun.* **151**, 272 (2003)
25. L. Verlet, *Phys. Rev.* **159**, 98 (1967)
26. S.A. Teukolsky, W.H. Press, *Numerical Recipes in C* (Cambridge Univ. Press, New York, 2002)
27. F. Piazza, Y.H. Sanejouand, *Phys. Biol.* **5**, 026001 (2008)
28. R. Castelli, M. Gameiro, J.P. Lessard, [arXiv:1509.08648](https://arxiv.org/abs/1509.08648) (2015)
29. E.J. Doedel, R.C. Paffenroth, H.B. Keller, D.J. Dichmann, J. Galan-Vioque, A. Vanderbauwhede, *Int. J. Bifurc. Chaos* **13**, 1353 (2003)
30. J. Moser, *Commun. Pure Appl. Math.* **29**, 727 (1976)
31. A. Weinstein, *Inv. Math.* **20**, 47 (1973)